

A study on the limits and advantages of using a desktop cutter plotter to fabricate microfluidic networks

Monsur Islam, Rucha Natu and Rodrigo Martinez-Duarte*

Multiscale Manufacturing Laboratory. Department of Mechanical Engineering, Clemson University, 29634, USA.

Abstract: In this paper, we focus on characterizing the limits of xurography, or patterning with a razor blade, of a pressure-sensitive double-sided adhesive. This is a rapid, inexpensive technique to fabricate robust microfluidics devices. Straight, curved and square serpentine as well as zigzag channels of different dimensions are studied. General guidelines are provided to assess feasibility of a particular geometry *a priori*. The mechanics of the cut are explored with the aim at identifying the bottlenecks that limit the maximum resolution achieved in xurography of adhesive films. A number of advantages and disadvantages of this technique compared to other common fabrication techniques are also provided.

Keywords: Cutter plotter, inexpensive, Xurography, disposable microfluidics, Gradient generator, Microchannel, Pressure sensitive adhesive

* Corresponding author: rodrigm@clemson.edu

1. Introduction

Microfluidics has become one of the most researched areas in the scientific community because of its wide range of application, from molecular biology to fuel cells (Whitesides 2006; Choi et al. 2012; Mu et al. 2013). Many ideas are being implemented by researchers from many different backgrounds and thus, the demand for a low cost, flexible and quick process to fabricate microchannels keeps increasing.

Historically, the majority of the initial microfluidics work was done using glass- or silicon-made microfluidic devices (Harrison et al. 1992; Wilding et al. 1994; Woolley and Mathies 1994; Jiang et al. 1995) using techniques like wet and dry etching. In the mid 90's, a revolution in the fabrication of microfluidics took place with the advent of soft lithography, where a master mold is used to make poly-dimethylsiloxane (PDMS) replicas by casting (Dong et al. 1996; Xia and Whitesides 1998; Duffy et al. 1998). Soft lithography is now a standard for microfluidic prototyping, in part because it enables a relatively inexpensive and rapid fabrication. As long as a master mold is available, experimental microfluidics devices can be made in few hours without the need for a cleanroom. However, the master molds are still mostly fabricated in a cleanroom following a number of processes including dry etching of silicon and especially SU-8 photolithography (Martinez-Duarte and Madou 2011). As expected, the resolution and achievable complexity of the master mold depend highly on the choice of fabrication technique. For example, microchannels with features of even 100 nm are possible to fabricate using electron beam lithography (Rogers and Nuzzo 2005; Alom Ruiz and Chen 2007). However, most microfluidic devices would feature dimensions from the tens of micrometers to several hundreds, achievable with conventional SU-8 photolithography.

Other relatively inexpensive fabrication techniques are printer-based, such as that presented by Carrilho *et al.* who selectively deposited hydrophobic wax on regular paper to create channel walls (Carrilho et al. 2009). In this particular case, the cross section of the channel is not empty but contains fibers that facilitate the wicking of the sample throughout the fluidic network. Bruzewick *et al.* also demonstrated a printer-based approach when using a desktop plotter to fabricate microfluidics channels on filter papers with a modified pen filled with PDMS (Bruzewicz et al. 2008). Yi *et al.* used a laser printer to cut microchannels from hydrophobic paper and sandwiched the paper into two glass slides to fabricate a device (Xin Yi, Rimantas Kodzius, Xiuqing Gong, Kang Xiao 2010). Munson and Yager fabricated a microfluidic mixer with polymeric laminates (Munson and Yager). They used CO₂ laser printer to pattern microchannels out of sheets of Mylar® or pressure sensitive adhesive-coated Mylar. They then laminated the layers using a custom-built jig.

Xurography refers to patterning using a razor blade. The term was introduced in 2005, when Bartholomeusz et al. presented the patterning of different materials using a cutting plotter, and their application in electroplating, shadow masking, PDMS micromolding and laminated microfluidics (Bartholomeusz et al. 2005). Since then, a number of microfluidic devices have been implemented using this technique (for example Nath et al. 2014, Pjescic and Crews 2012, Greer et al. 2007, Atencia et al. 2012, Kido et al. 2007, Gorkin et al. (2010)), including several works by our group (Martinez-Duarte et al. 2011, Martinez-Duarte et al. 2010, Martinez-Duarte et al. 2013). The use of xurography to pattern adhesive films has been particularly meaningful to the microfluidics community since robust, inexpensive devices can be fabricated in matter of minutes without the need for a cleanroom. Here, we present a study on the accuracy and precision that can be expected when fabricating common microfluidics structures with a relatively inexpensive cutter plotter. To the best of our knowledge no thoroughly and systematic characterization of the limits of this technique has been presented. For example, Bartholomeusz et al. reported a number of cuts below 150 μm using different film thicknesses, but such features feature poor accuracy, averaging 20% of the targeted value as difference from the targeted dimensions, and poor precision, up to 25.9% discrepancy between similar cuts (Bartholomeusz et al. 2005). Yuen and Goral reported a limit of 200 μm when cutting serpentines from a 50 μm -thick pressure sensitive adhesive, but without reporting the degree of precision and accuracy and only targeting curved serpentines (Yuen and Goral 2010). Do and colleagues briefly reported on the effect of cutting force on the width and depth of single-line scratches, not through cuts, made in a 1 mm-thick cyclic olefin polymer. Their application was to engineer the surface of the COP and use it as channel top and bottom (Do et al. 2011). More recently, Cosson and colleagues reported high accuracy (98.7% average) when cutting patterns above 100 μm in 150 μm -thick PDMS films (5:1 elastomer to

curing agent) (Cosson et al. 2015). From the existent literature, a fuzzy limit between 100 and 200 μm seems to exist regardless the choice of material, thickness, and equipment. The purpose of this work is to study the precision and accuracy achievable with xurography when cutting straight, curved and square serpentines, and zigzag channels of different dimensions. We are aware that the exact limit depends on the specific cutter plotter and material used in each case, but we aim at envisioning physical constraints that would limit a cutting operation. Furthermore, we believe the cutter plotter used here is representative of commercial inexpensive plotters that could be considered affordable by many, and the materials studied are also representative of double-sided pressure-sensitive adhesives (PSA) that would be mostly used in the fabrication of microfluidics devices. The patterning of metal films is not within the scope of this work. The fabrication set up we used, a cutter plotter plus a laminator, has an estimated cost below USD\$2,000 and does not require a cleanroom at any point. Furthermore, master molds, plasma treatment of the substrate, degassing of the polymer and heat treatment to crosslink it, are not necessary. The cost of PSA can be well below a US dollar per square foot. The protocol proposed is easy to implement and can enable extremely rapid and inexpensive prototyping of microfluidic designs. The whole process, from idea to implementation, can be as short as minutes. The main contribution of this work is to clearly identify the limits of the technology and provide general guidelines to the designer of common microfluidic geometries. We first present the characterization of such geometries, followed by the determination of the robustness of the film under fluid pressure and chemical exposure. At the end we detail a number of advantages and disadvantages of this fabrication technique as well as few practical recommendations.

2. Materials and Methods

2.1 Pressure-Sensitive Adhesive (PSA)

The double-sided PSA film used here is comprised of a polyester (PET) film, with low surface energy and high glass transition temperature, stacked between two layers of a polymer with high tackiness and low glass transition temperature. This PSA film is contained between two liners, a thin top liner to protect it from the environment and a thicker bottom liner that serves as the substrate during cutting. In this work, cuts are made only through the top liner and the PSA film. The thicknesses of both the PET and the adhesive layer in the PSA vary depending on the choice of product. The following PSA films were obtained from FLEXcon and were used as provided: FLEXmount® Advantage Value FAD, with a total thickness of 50 μm , Switchmark 212R, with a total thickness of 127 μm (25 μm of polyester and 48-53 μm of adhesive layer on each side), and Switchmark 272, 275 μm -thick (same thickness of adhesive layers but 178 μm -thick polyester film). The reasons behind choosing PSA as a material for microchannels include: 1) PSA films are inexpensive, *i.e.* a square foot of FLEXcon Switchmark 212R PSA (127 μm thick) can be well below a dollar. 2) Patterning of the PSA can be straight forward using a cutter plotter. 3) No heat is needed to activate the adhesive, so assembly can be done at room temperature. 4) The adhesive industry (for example FLEXcon and Adhesives Research Inc.) is quite developed, offering a wide variety of adhesives in terms of material, texture, doping and electrical conductivity which opens the possibility to integration of other functions, such as electrodes and surface morphology.

2.2 Channel Designs

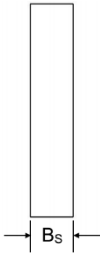
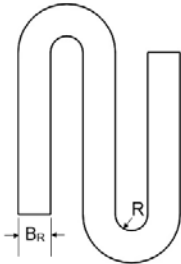
Straight, curved and square serpentines, as well as zigzag channels are studied here. Such geometries were chosen due to their common use in many lab-on-a-chip and microfluidics devices. For example, straight channels are common in electrophoresis and dielectrophoresis applications (Ai et al. 2009; Martinez-Duarte et al. 2013); zigzag channels for mixing (Ren and Leung 2013); curved serpentine channels for particle separation (Cho et al. 2007) and square serpentines channels can be used for bubble transport (Cubaud and Ho 2004). We characterized each of these designs based on the parameters shown in Table 1: 1) For straight channels, the width of the channel (B_S); 2) for curved serpentine channels, their width (B_R) and radius of curvature (R); 3) for zigzag channels, their width (B_θ) and their angle of aperture θ ; and 4) for square serpentine channels (90° corners), their width (B_D) and the spacing between the arms (D). The range of values for each of these parameters is also shown. All channel geometries were designed using Solidworks (Dassault Systems, Waltham, Massachusetts, USA) due to availability and expertise. Other software such as Pro/Engineering, PTC Creo


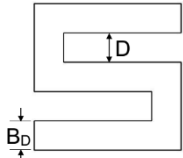
Parametric, CATIA, Adobe Illustrator and AutoCAD, could be used as long as a file compatible with the cutting plotter, in our case a .dxf file, can be generated.

2.3 Device Fabrication

The fabrication process is illustrated in Fig. 1. A cutter plotter (Graphtec CE6000-40, Japan) sitting on a laboratory bench was used to pattern the double-sided pressure-sensitive adhesive (PSA). A cutter plotter closely resembles an inkjet printer, but the print head is replaced with a cutting blade. The blades used in this work featured an angle of 30° or 45° and were used as supplied (Graphtec part number CB15U and CB09U respectively). The cut to be performed in this particular cutter plotter model is defined by four parameters: force, velocity, acceleration and offset. The force was varied depending on both the blade used and the thickness of the film to be cut. After an optimization process (data not shown), a force of 0.99 N for 50 μm , 1.88 N for 127 μm and 2.76 N for 275 μm thick adhesive was used when the cut was done using the 45° blade. When using the 30° blade, the force was reduced to 0.64 N for 50 μm , 1.17 N for 127 μm and 2.38 N for 275 μm thick adhesive. These force values were found to be the minimal ones to enable complete cutting through the top liner and PSA film, but not through the cutting liner. The use of less force leads to an incomplete cut, *i.e.* the PSA pattern cannot be fully released from the liner. Velocity, acceleration and offset were kept constant in all cases at 1 cm/s, 1 cm/s^2 and zero, respectively. A laser cutter (Epilog Laser Helix, Epilog Laser, USA) was used to fabricate the substrate and top cover of the device out of 2.38125 mm-thick ($3/32''$) cast acrylic sheets (McMaster-Carr #8560K181). Other materials such as polycarbonate and polyester could be used instead of acrylic, using appropriate patterning techniques. The laser cutting parameters for acrylic were optimized (data not shown) to achieve inlet and outlet ports with diameter slightly wider than 1.5875 mm ($1/16''$). Once all individual PSA and acrylic parts were made, they were aligned using dowel pins and alignment holes in each of the layers, stacked together and manually pressed to stick them together. The stack was then fed through a roll pressure laminator (JetMounter, DRYTAC, USA) to activate the adhesive and seal the microfluidics network.

Table 1: Geometries of interest in this study, their characterizing parameters and the range of values studied for each

Figure of the Channel	Type of Channel	Parameter	Range (μm)
	Straight Channel	Width B_s	200 to 1000
		Radius of Curvature R	200 to 1500
		Width B_R	200 to 1000

	Zigzag Channel	Angle of aperture θ	30° to 165°
		Width B_θ	200 to 1000
	Square wave Channel	Distance between horizontal arms D	150 to 2400
		Width B_D	200 to 1500

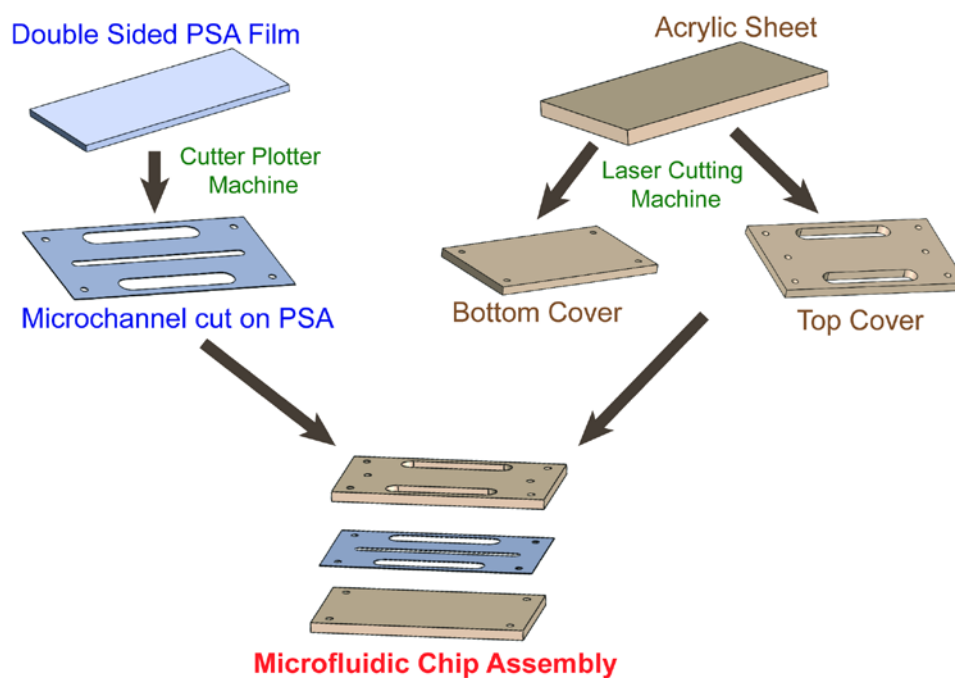


Fig. 1: Schematic of the entire fabrication process of the microfluidic chip

2.4 Characterization of Microchannels

After assembly, characterization was done using a Nikon Eclipse LV100 microscope using 10X and 20X objectives. Measurements were done using the native microscope software (NIS Elements Basic Research). A minimum of five samples per channel design were characterized. In straight channels, width was measured at both ends and at the middle of the channel. For the serpentine channels, measurements of the width were performed at the two ends and at the curvatures. The radius of curvature was measured directly in the curved region and also as the gap between two horizontal regions of the channel. In the zigzag and square channels, the width of the channel was measured on both ends and on the square or zigzag. The angular measurements for zigzag and the spacing D in square channels were taken as the angle or spacing between the internal walls of the two branches, respectively. In total, five measurements were performed for each sample channel that was cut.

2.5 Experimental Protocol to determine reliability under pressure

To investigate the behavior of PSA film under pressure, closed chambers were fabricated with 127 μm thick PSA and acrylic using the fabrication method detailed above. In this case, rings of different thicknesses: 1, 2, 4, 8 and 16 mm, were cut and positioned on top of a flat acrylic piece. The chamber was closed and sealed using an acrylic cover that featured only one hole. The assembled device is illustrated in Fig. 6a. The test chamber's only access port was connected to a syringe pump (FusionTouch 200, Chemyx, USA) using flexible tubing (1520, Upchurch Scientific/IDEX, USA). The tubing was bonded to the chip using generic epoxy glue to guarantee that the weakest point in the test setup is the PSA film. The pressure in the line between the test chamber and the syringe pump was monitored throughout the experiment using a pressure sensor (LabSmith uPS0800-C360-10 with range 0-800 kPa). The integrity of the PSA ring was monitored using a digital microscope (Dino-Lite AM4815ZT). Water dyed with red food color was pumped continuously into the test chamber at $Q=500 \mu\text{l}/\text{min}$ until the PSA started to peel (developing fingers from the chamber inner edge) and eventually busted in some cases. Three experiments were performed for each of the ring thicknesses.

3. Results and Discussion

3.1 Straight Channel

The results obtained when cutting straight channels of different width B_s are shown in Fig 2 and Table 2. Solid black circles and blue rectangles depict feasible cuts using blades with 45° and 30° angle respectively. Red triangles illustrate failed cuts. A cut was classified as failed when no clear separation between the edges of the channel was seen. As such, attempted cuts with channel width below 200 μm were not achieved. Although the resolution of the plotter used in this work is 25 μm it appears other parameters must be taken into account to determine the practical resolution.

Table 2: Targeted dimensions vs. average measured dimensions for different channel widths and blade angles. Adhesive thickness was 127 μm . Data plotted in Fig. 2.

Targeted Dimension (μm)	Average Measured Dimension (μm)	
	45° Blade	30° Blade
1000	997.22 \pm 2.83%	1004 \pm 1.82%
900	907.3 \pm 4.15 %	903.66 \pm 2.07%
800	807.1 \pm 4.66%	806.39 \pm 2.92%
700	705.22 \pm 4.75%	704.42 \pm 2.65%
600	599.32 \pm 5.5%	605.51 \pm 2.69%
500	510.75 \pm 7.78%	499.48 \pm 2.78%
400	410.97 \pm 9.97%	406.48 \pm 4.52%
300	316.61 \pm 22.8%	295.34 \pm 5.9%
250	287.14 \pm 23.8%	251.3 \pm 6.98%
200	231.84 \pm 26.5%	208.07 \pm 9.09%

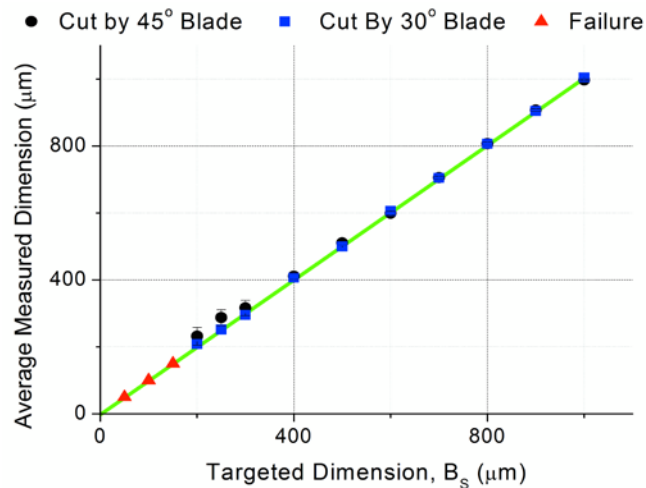


Fig. 2: STRAIGHT CHANNEL. Average dimensions achieved when cutting channels with different widths on 127 μm -thick PSA film using different blades. Black circles and blue squares depict successfully-cut channels while red triangles indicate unsuccessful attempts. The diagonal bar reflects completely accurate cuts. Bars indicate the percentage error with n at least 5

Accuracy of the cut appears to be independent from the choice of blade only when cutting channel widths above 700 μm . The use of the 30° blade yields clear benefits in terms of accuracy when cutting channels narrower than 700 μm . The precision of the cut depends on the blade angle as shown in Table 2. For each dimension, the percentage error is less for the cuts using the 30° blade than those done with the 45° blade. The impact of the choice of blade angle on precision is most severe when cutting the narrowest channels. The percentage error for 200 μm channel cut by 45° blade is as high as 26.5%, whereas with 30° blade the percentage error comes down to 9.09%. The first parameter that comes to mind when attempting to explain these dimensional errors is the resolution of the machine. In our case this resolution is 25 μm , as provided by the manufacturer, which has been found to be representative of plotters in the same price range. More expensive plotters can feature a resolution of 10 μm . However, our results show that the practical resolution is far from this value. We suspected the geometry of the blade to be the next important factor. The blades used in this work are of the drag knife type, meaning the blade swivels in its holder and is automatically oriented with the direction of the cut. This is good since the cutting edge is always aligned to the cut but the fact that the blade is floated limits the rigidity of the blade during cutting, which may lead to dimensional error. Microscopic examination of both blades illustrates a metal cylinder (~2.5 mm in diameter) which tapers into a triangular prism on its cutting end. This triangular prism ends on a flat with the cross-section of an isosceles triangle with measured base of 47.28 μm , height of 61.49 μm and sharpest angle of 42°. Thus the footprint of the blade during cutting is an effective 47.28 μm . The angle (30° or 45°) stipulated by the manufacturer is actually the taper angle of the cutting edge, the line connecting the sharpest point of the isosceles triangle to the circular cross-section, with respect to the back of the triangle. For a 30° blade the length of the cutting edge is 1.5 mm, which decreases to 865 μm in the case of a 45° blade. Although the resolution of the machine is 25 μm , the footprint of the blade is well above that: a 47.28 μm to cut an extremely thin film, but increasing according to the taper angle. For example, at the top of a 127 μm -thick film, the footprint of the 30° and 45° blades is 103.27 and 144.70 μm respectively. These calculations were made assuming the shape of the triangle is maintained and just scaled up throughout the taper of the blade. These results suggest that the geometry of the blade can be held accountable for the practical limit of 200 μm in the case of the 30° blade and 300 μm in the case of 45° blade. Note how above these limits the accuracy of the cuts is within less than 10 μm of the desired value.

Another factor that must be taken into account is the orientation of the cut with respect to the plotter. All the cutter plotters we are aware of feature a cartridge-like module that holds the blade and is mounted on a rigid rail. The film, or workpiece, is rolled back and forth under the blade using spring rollers. Thus, the blade only moves in one direction, let's say X. The other cutting direction, Y, is implemented by rolling the film back and forth. The mechanics of movement are not the same in X and Y. During a straight cut in X, the blade is moved along the rigid rail to cut a stationary film. The cut benefits from a more controlled movement with possibly better resolution. During a straight cut in Y, the (thin, flexible) film is pushed against a stationary blade. Two observations are important: 1) during a straight cut in either X or Y one of the motors remains off, eliminating

one degree of uncertainty in the process; and 2) the quality of the cut in X is higher than in Y, as also noted by previous authors using a different cutter plotter (Yuen and Goral 2010).

Finally, we also hypothesize the blade tip collects debris from the cut layers of PSA. As adhesives are sticky, the debris adheres to the blade tip which effectively changes the geometry of the blade. This is similar to a build-up edge in a machining operation where material collected on the tip effectively changes the cutting angle of the tool leading to surface roughness and loss of precision.

3.2 Curved Serpentine channels

At this point is important to mention that for the rest of this work, a cut was considered failed if its dimensional deviation exceeded the dimensional error presented in Table 2 for each targeted dimension. For example, a 200 μm -wide serpentine channel cut with the 30° blade was considered a failed cut if its dimensional error was more than 9%. Accordingly, error bars are not shown in the data points of the plots below since they are below the values reported in Table 2 and because they will add unnecessary complexity to the plots. Although some serpentine and zigzag channels can be physically cut, their dimensional error throughout their length would be big enough to hinder their use in an experimental device.

The results obtained when characterizing the fabrication feasibility of serpentine channels in a 127 μm -thick PSA film are shown in Fig. 3a. The serpentine channels are oriented parallel to the X axis of the cutter plotter to take advantage of the better cut quality in the X axis. This study was started at channel widths of 200 μm , based on the practical limit determined when cutting straight channels. Although better cuts are obtained using the 30° blade, both blades are characterized to determine under which situation the 30° blade is an absolute necessity, since it is more expensive than the 45° one. Different radii of curvature were explored, ranging from 200 to 1500 μm . Symbols illustrate three different cases: failed cuts (red triangles), cuts achieved using either blade angle (solid black circle) and cuts only achieved using the 30° blade (blue squares). It was expected that 200 μm -wide channels with 200- μm radius of curvature would be successfully cut, given previous results with straight channels. Unfortunately, this was not the case. Indeed, the designer must make a compromise between channel width and radius of curvature. Smaller channels only allow for wide radii of curvature. For example a 200 μm -wide channel only allows for radius of curvature above 1000 μm . Interestingly, curvature radii below 300 μm were not achieved at any channel width. The lowest radius of curvature achieved within the specified dimensional error was around 300 μm but only when the channel width is wider than 600 μm . The green curve was empirically fitted to the points at the boundary between failed and feasible cuts and is given by Equation 1. Above this curve, all the cuts are defined as feasible and featuring a dimensional error equal or less than that reported in Table 2. This empirical formula would prove a valuable design tool for the fabrication of feasible channels when using xurography of PSA films like those described here and attempting cuts in the range of values presented in figure 3a

$$R = 9.54 \times 10^4 \times B_R^{-0.86} \quad \text{Equation 1}$$

For channel widths below 300 μm , it was common that the two lines defining the channel walls were merged into a single line at the curved portion of the geometry. Although the resolution of the machine is high enough to plot curved lines with radius of curvature around 300 μm , the mechanics of the cutting operation seem to prevent cutting of uniform channels. As previously mentioned by other authors, a minimal dimension exists where the bonding strength of the film to its cutting liner, given by the bonding area, is surpassed by the lateral force of the blade acting on the film. At this point, the adhesive film moves. Such movement led to an inaccurate cut or in the worst case, the blade peeled the PSA film, effectively creating a physical obstacle that hindered the continuity of the cut. Enough bonding area must be present to sustain the force exerted by the blade on the film during cutting, hence the trade-off between the width of the channel and the radius of curvature. If both are small, the blade trajectories are too close to each other leaving little bonding area between them. A PSA film with stronger adhesion to the liner may be a solution towards achieving sharper radii of curvature in narrow channels. However, a compromise must be met since the patterned PSA film must be easy to remove from the cutting liner. Other PSA formulations may feature an optimized value in this respect.

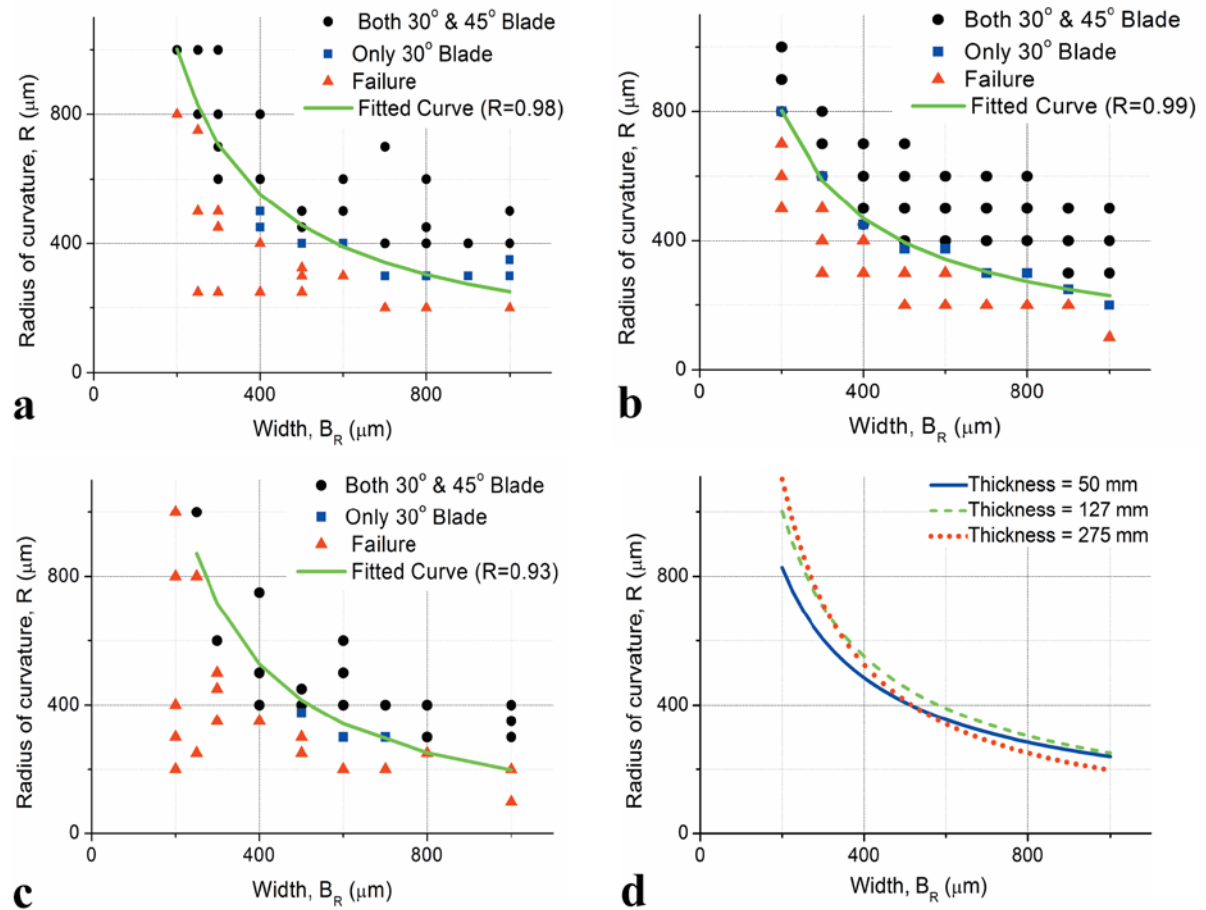


Fig. 3: SERPENTINE CHANNELS OF VARYING THICKNESS. Relation between width of the channel and Radius of curvature of the serpentine geometry for (a) 127 μm thick PSA film, (b) 50 μm thick PSA film, (c) 275 μm thick PSA film. n at least 5. (d) Plot showing the fitted curves obtained in (a), (b) and (c) together. Fitted curves are those with highest R among different fits attempted in Matlab 2014a. These curves are only valid as guidelines over the range of values presented in the figure.

3.3 Zigzag channels

The results characterizing the fabrication of zigzag channels are shown in Fig. 4. The types of data points presented are similar to those detailed in the section above. The zigzag geometries were oriented in such a way that if one were to stretch the zigzag into a straight channel, this channel will be perpendicular to the X axis. The angles of aperture studied included 30, 45, 60, 90, 120, 150 and 165°. The sharpest angle, 30°, was only achieved when the width of the channel was equal to or more than 300 μm . A 200 μm channel width can only be obtained when the aperture angle is wider than 60°; a single line was obtained when attempting sharper angles. The threshold between feasible and non-feasible cuts in the range of values presented in fig. 4 is determined by the empirically fitted green curve, given by Equation 2.

$$\theta = 2.29 \times 10^6 \times B_{\theta}^{-1.85} \quad \text{Equation 2}$$

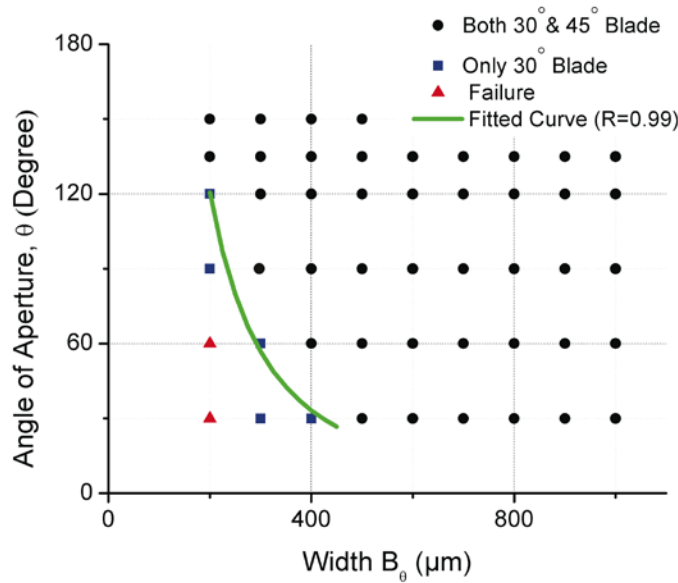


Fig. 4: ZIGZAG CHANNEL. Relation between the width of channel and the angle of aperture in a zigzag channel for 127 μm thick PSA film. n at least 5. Fitted curve with highest R among different fits attempted in Matlab 2014a.

Interestingly, sharp features, $\theta=30^\circ$, can be fabricated with channels as narrow as 300 μm . The question arises about the reason why such features can be cut as zigzag but not as a sharp radius of curvature in a serpentine. We hypothesize is because the lateral force exerted by the blade is less when cutting straight lines, as in a zigzag, than when cutting a curve, as in the serpentine. Coincidentally, Cosson et. al. have recently demonstrated the cutting of openings as small as 25 μm when cutting a triangle, basically a V-shaped incision, into one of the edges of a square.

3.4 Square Serpentine channels

The dimensional limits for square wave channels are shown in Fig 5. Similar to the previous channels, three kinds of results were obtained: successful cuts by both of the blades, successful cuts by only 30 $^\circ$ blade and failed cuts by using any blade. The minimum channel width that can be achieved in these square geometries is 300 μm , but only if the spacing between branches is above 1.5 mm. Alternatively, a minimum spacing between branches of 300 μm is only achieved if the width of the channel is as wide as 1.5 mm. Similar to the cases of serpentine and zigzag channel, the empirically fitted threshold curve is plotted as a green curve described by Equation 3.

$$D = 2.44 \times 10^5 \times B_D^{-0.89} \quad \text{Equation 3}$$

The blade tends to peel off the PSA film at sharp corners while cutting channels with small distance between arms. This reinforces the theory that the bonding strength between the film and its cutting liner must be greater than the force exerted by the blade to avoid film movement. To this end, it is interesting to compare the case of square serpentine and a zigzag with a 90 $^\circ$ angle of aperture. The corners are similar but the bonding area of the cut pattern is different. A cut pattern with 3 exposed edges only arises when cutting a square serpentine, in contrast to two exposed edges when cutting a 90 $^\circ$ zigzag. The former severely undermines the bonding strength of the film to the liner. Furthermore, a square cut is the most extreme in terms of force acting on the film, as the force is perpendicular to the film edge. Hence the stricter limitation on the achievable square serpentine dimensions when compared to curved serpentine, zigzags and straight channels. Analyzing the results obtained in the last four sections one may conclude that the most viable way to achieve small structures using xurography is by implementing straight cuts, followed by zigzags, curves or square cuts, in that order of preference. The

lateral force acting on the film is negligible when cutting straight lines. It increases when cutting slant straight lines and curved features, while it is most when implementing square serpentine.

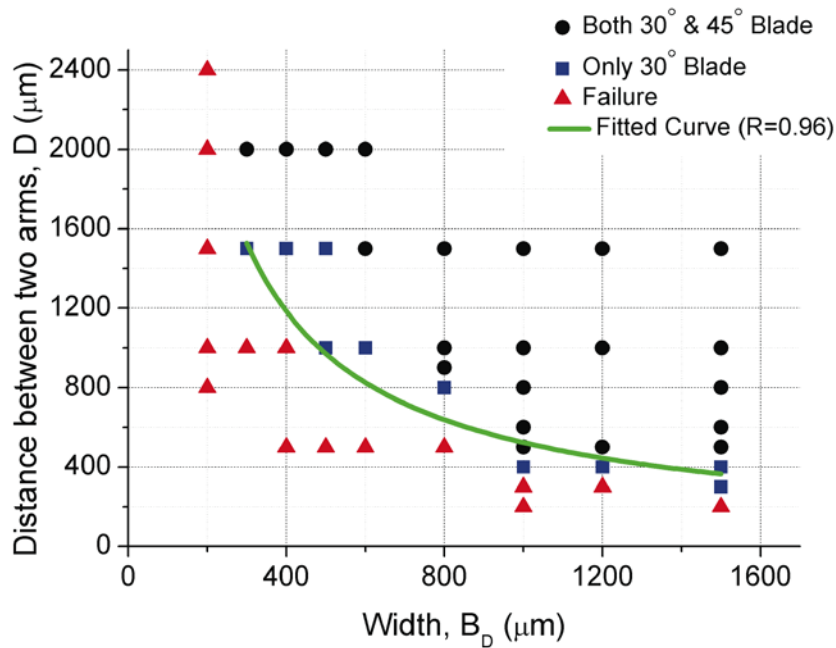


Fig. 5: SQUARE CHANNEL. Relation between the width of channel and the square gap of the square wave channels for 127 μm thick PSA film. n at least 5 for each data point. Fitted curve with highest R among different fits attempted in Matlab 2014a. The empirically fitted curve given by equation 3 is valid only in the range of values presented in the figure.

3.5 Variation with thickness

Bartholomeusz et. al. postulated that the thickness of the film has an impact on the smallest feature that could be achieved in xurography. The analysis of the blade geometry detailed above also reinforces the principle that the thinner the film, the higher the resolution that can be achieved. In this section we present the results when cutting 3 films of different thicknesses. Curved serpentine of different dimensions were attempted on 50 μm -thick PSA (FLEXmount® Advantage Value FAD) and 275 μm -thick PSA film (FLEXcon®Switchmark 272) to complement the results obtained when patterning the 127 μm -thick film. Curved serpentine were chosen given their intermediate standing in terms of lateral force acting on the film, relative popularity in the community and the fact that changes on both channel width and radius of curvature can be studied. The 50 μm and 127 μm -thick PSA films could be cut in a single blade pass, but the 275 μm -thick adhesive required at least two blade passes. The results are shown in Fig. 3b and c. The best empirically-fitted curves for 50 μm and 275 μm thick PSA follow Equation 4 and Equation 5 respectively.

$$R = 4.89 \times 10^4 \times B_R^{-0.77} \quad \text{Equation 4}$$

$$R = 3.18 \times 10^5 \times B_R^{-1.069} \quad \text{Equation 5}$$

To facilitate the comparison between the results obtained with different film thicknesses the best fits to the experimental data of Fig. 3a, b and c are plotted together in Fig. 3d. At first sight the curves seem to overlap, leading to the conclusion that thickness does not play a role on the achievable dimensions. However, closer examination does reveal that the use of thinner films enables a slight increase in performance. Although curvature radii equal or below 200 μm were not achievable with any film thickness, it can be seen that the curves shift slightly to the right as the PSA thickness increases. Channels featuring 200 μm width and radius of curvature of 800 μm were only possible in 50 μm PSA films. Only when the radius of curvature is equal to 1 mm is when channels widths of 200 μm are possible in 127 μm -thick PSA. 200 μm -width channels are not

possible in 275 μm film regardless of the radius of curvature. Since patterning of the thicker film required more than one pass, the cutting zone that results from several passes features a width close to 200 μm . Hence, the two lines which define the channel wall merge together and the channel having 200 μm width comes out as a single line instead of a channel. Another interesting fact is that channels with radius of curvature equal to 200 μm are only achievable in 50 μm films. For features with 200 μm radius of curvature, failure occurs in 127 μm and 275 μm thick PSA due to dimensional error. Hence, the thickness of the film plays a small but important role in the determination of the achievable resolution when cutting PSA films.

3.6 Device Robustness

In this section we present the characterization results of the PSA behavior under pressure and when in contact with different chemicals.

The test chamber used for pressurized experiments is shown in Fig. 6a and detailed above. After applying the epoxy glue at the inlet, the adhesive ring was deemed to be the weakest point in the test chamber. As dyed water was continuously forced into the test chamber, the pressure increased until the ring started peeling and eventually busted open and water leaked. We focused on the peeling pressure, which is the pressure value when the PSA started peeling from the substrate and finger-like patterns started appearing at the inner edge of the chamber. We assume the peeling pressure to be the maximum pressure the adhesive can withstand and these values are reported in Fig. 6b for different ring thicknesses. We also recorded leakage pressure, which is when these finger-like patterns connected both edges of the adhesive ring and water could leak out of the chamber. The peeling pressure of a 1 mm-thick ring is just under 100 kPa. As expected, the peeling pressure increases according to the ring thickness. Perhaps intuitively the designer would be inclined to include a surrounding band as wide as possible to seal a microfluidics network. However, thicknesses beyond 8 mm do not offer any improvement on the maximum pressure (325 kPa) that can be sustained. In fact, when using this particular adhesive a 4 to 8 mm-thick band would be sufficient to surround the microfluidics network. This is an important design parameter to exploit all the real estate available on a substrate. One must then model the pressure gradient in a particular structure at a given flow rate and assure that the maximum pressure does not surpass the peeling pressure of the PSA. While the numerical result presented here is particular to this PSA film, an optimal thickness of the surrounding band is expected to exist for other PSA films. This optimal thickness would depend on the ultimate peel constant of a particular PSA to a specific substrate. Besides the choice of substrate, this constant depends on the film thickness and its formulation. Counter intuitively, the dependence is not always proportional to the film thickness. For example, the 127 μm -thick PSA film used in this particular section features an ultimate peel constant of 671 N/m to polycarbonate and 306 N/m to ABS (<http://www.flexcon.com/ProductsSolutions/Brands/Products/>). The 275 μm -thick PSA detailed above features an ultimate peel constant of 1430 N/m to polycarbonate but only 286 N/m to ABS. Regarding leakage pressure, the test chambers with the PSA width of 4, 8 and 16 mm did not burst within the pressure range that could be studied (up to 800 kPa), whereas test chambers with 1 and 2 mm-wide PSA busted at 411.533 kPa and 764.406 kPa respectively. A practical concern when fabricating these devices is the bubble density that is introduced during film lamination. Bubbles represent a weak spot in the film and the lower the density the stronger the film.

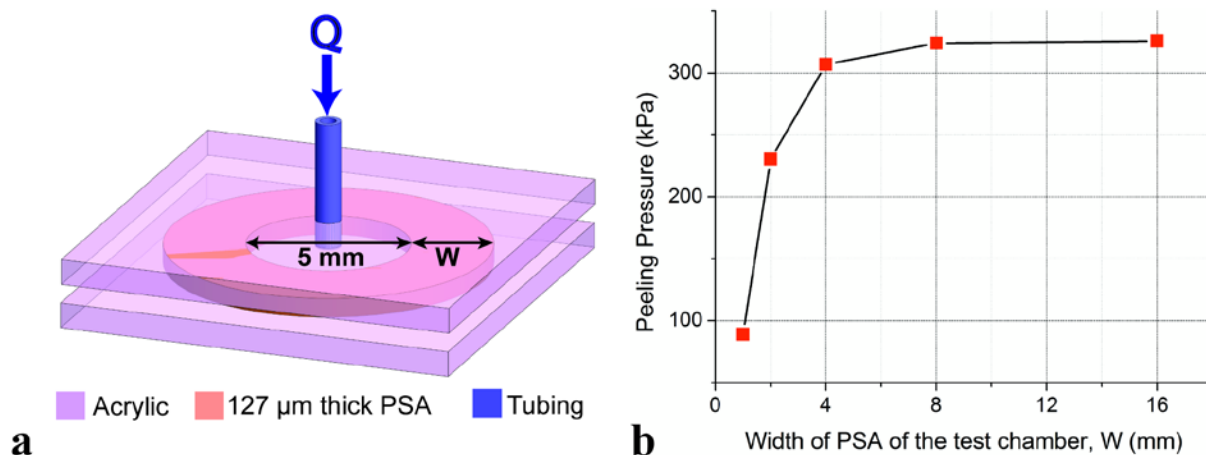


Fig 6: (a) Test chamber used to investigate the behavior of PSA under pressure; (b) The peeling pressure obtained for different thickness of the PSA ring, see text for details.

Chemically, the microfluidic chip assembly is inert to a number of media commonly used in lab-on-a-chip applications. The assembly presented here has been tested with solutions of sugar, bovin serum albumin (BSA), phosphate buffer saline (PBS), sodium dodecyl sulfate (SDS) and isopropyl alcohol (IPA). Leaching studies have not been performed by us or by the manufacturer of this particular adhesive and may be necessary for some applications. However, a number of PSA films have been used for PCR, DNA and electrophoresis applications with good results, for example those by (Nath et al. 2014), (Pjescic and Crews 2012) and (Greer et al. 2007). Solvents do attack both the adhesive film and a number of plastics. However, IPA can be flowed for a minute to clean the fluidic network without a noticeable etch. Exposing the adhesive to IPA for prolonged periods causes the adhesive to dissolve. In fact, introducing the assembled chips in an IPA bath for up to 72 hours completely dissolves the adhesive, enabling the re-use of the acrylic covers and substrate. The use of acetone is not recommended, since acetone will also attack the acrylic cover and substrate. Beside acrylic, other polymers can be used in the device such as polycarbonate and polyester.

3.7 Advantages and Disadvantages

Although the inexpensive patterning technique detailed here cannot achieve dimensions below 300 μm with high precision, it provides several important advantages when fabricating structures with dimensions above this limit. Perhaps the most important one is that it enables implementation of a design in just few minutes using relatively inexpensive resources. The devices demonstrated here are robust and capable of handling high-pressure gradients. Fabrication can be done in a common room, no need for a cleanroom. The infrastructure needed, a cutter plotter and a laminator or rolling press, can be quite inexpensive (below USD \$2000 at the time of publication). This technique can be a viable alternative to soft lithography when fabricating relatively big structures. The desired shapes can be directly made without the need for master molds, polymer degassing or plasma treatment. SU-8 photolithography of thick structures (> 100 μm) can be hours-long and cumbersome, and the technique proposed here can significantly shorten fabrication time. If PDMS must be used as the channel material, this technique could also allow for the fabrication of a mold; by adhering the shape to replicate to a substrate (data not shown). In terms of material, PSA films can be inexpensive, in the order of tens of cents (USD) per square foot. Furthermore, the PSA industry is constantly introducing different attributes to their films including adherence strength, electrical conductivity, texture, thickness and dissolvability. Importantly, the PSA film can be dissolved away using mild solvents such as IPA, which enables the re-use of the substrate and polymer covers.

Regarding disadvantages, the most important one is perhaps the roughness of the channel walls, see Fig. 7. The quality of the channel walls depends on the cutting parameters. The best quality, which would still be considered rough by some, is achieved at low cutting speeds, such as those disclosed here. The cutting force should also be adjusted to only cut the top liner and the PSA film. Although the walls can be rough, they have not interfered in dielectrophoresis and centrifugal microfluidics experiments (Kido et al. 2007; Martinez-Duarte et al. 2013). Another potential disadvantage is the fact that a rolling press is used to seal the devices. This operation does not represent a problem when the substrates are based on polymers but can be challenging when using fragile substrates such as glass or silicon (Jaramillo et al. 2010; Mernier et al. 2012).

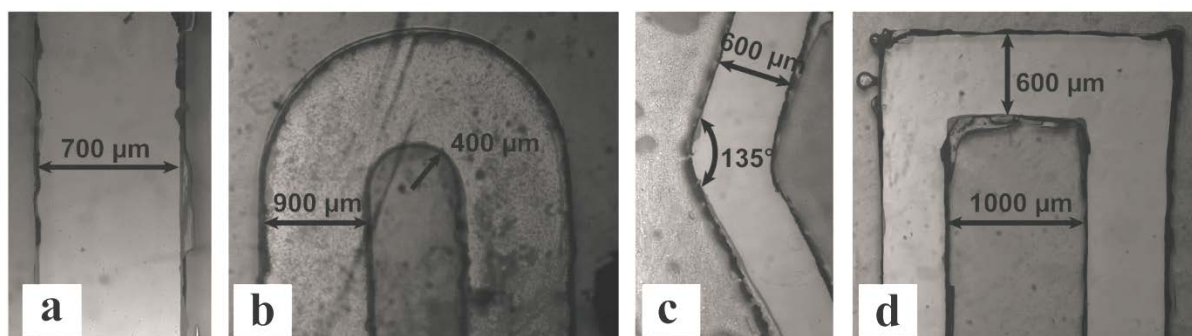


Fig. 7: Characteristic examples of wall roughness in (a) Straight, (b) Serpentine, (c) Zigzag, and (d) Square microchannels.

3.8 Further practical considerations

- When attempting to cut features below 300 μm , the cutter plotter is not able to cut a contour. Instead, two parallel lines can be designed following the desired channel geometry. The two parallel lines can then be joined by a manual cut or by two line cuts done by the machine.
- The cut quality of the PSA film also depends on the residual stress present in the film. Most of these films are manufactured and delivered in roll format. Flattening the film previous to attempting narrow cuts is recommendable.
- This fabrication method can be used with a variety of substrates, including silicon wafers, fused silica, alumina and common glass, bare or coated with SU-8. Care must be taken during the rolling press operation.
- Stacking of several layers of alternating adhesive, films and other materials is possible to achieve complex 3D fluidics.

3.9 Device validation as Microfluidic Gradient Generator

As detailed in the introduction, xurography has already enabled several microfluidic applications and further demonstration of the same functions in this work was considered unnecessary. Here we only present a gradient generator, as one good example of a complex microfluidic structure that can be fabricated with xurography. The device is shown in Fig 8a as fabricated from the 127 μm -thick PSA film detailed above. A gradient generator is a widely used tool in the microfluidics community, for example as cell culture systems as reviewed by (Keenan and Folch 2008). The design shown here features a width of individual serpentine channels of 680 μm and 680 μm -radius of curvature. The length of each serpentine is 10.84 mm. All serpentine channels merge into a main channel with width 2.75 mm and length 25 mm. After assembly, the experimental device was used to generate a gradient between yellow and blue-dyed fluids. A detailed view of the gradients in the region marked by the red rectangle in Fig 8a are shown in Figures 8b, 8c, 8d and 8e when flow rates at the inlets were 0.1, 1, 10 and 100

$\mu\text{l}/\text{min}$ respectively. The diffusivity of the gradient is inversely proportional to the flow rate in the channel. Very high flow rates hinder diffusion of the dyes between the streams and hence individual streams can easily be identified in those cases. Ongoing work is on studying the chemotaxis of parasites when exposed to different gradients in these devices.

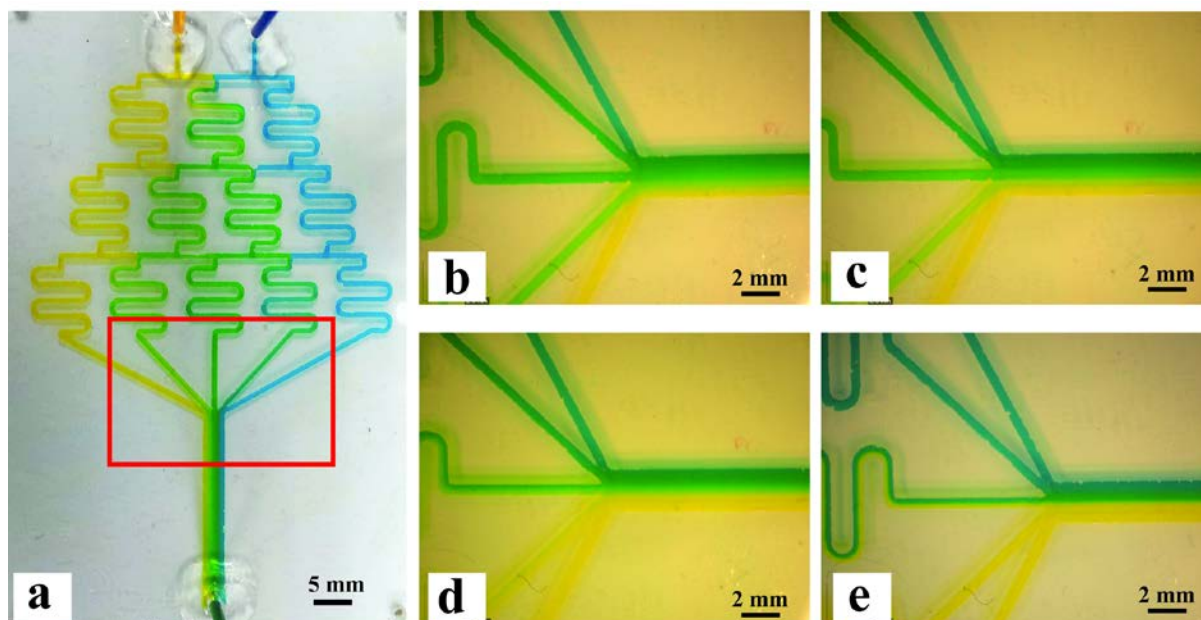


Fig. 8: (a) Design of the gradient generator and the gradient when flow rates are (b) $0.1 \mu\text{l}/\text{min}$, (c) $1 \mu\text{l}/\text{min}$, (d) $10 \mu\text{l}/\text{min}$ and (e) $100 \mu\text{l}/\text{min}$

4. Concluding Remarks

The main contribution of this work is clear identification of the limits of the fabrication technology presented, and provision of general guidelines to the designer. A combination of the different shapes studied here could be implemented in the development of rather complex microfluidic platforms, *i.e.* a combination of curves with zigzags and straight cuts. The smallest feature that can be achieved depends on the pattern to be cut. In all cases, a compromise is required between the width of the channel and the separation between channels. The angle of aperture or the radius of curvature can characterize the separation between channels in geometries other than square serpentines. Equations 1-5 are empirical fittings to the boundary between feasible and non-feasible cuts obtained by experimentation. These equations are valid as guidelines only in the range of values presented in their correspondent figures. Although these equations are particular to the specific infrastructure and materials used in this work, we believe them to be an acceptable general guideline for xurography of PSA films. This is because the factors identified to impede higher resolutions in this work are inherent to a cutting operation, regardless of the cutter plotter model and type of PSA. The specific resolution of the machine has been found to be marginally important since most of the cutter plotters that are commercially available feature resolutions well below the practical resolution found here and also reported by others. The blade geometry is suspected to be the main determinant of the cutting resolution. The development of a finer blade would be beneficial but it would likely come with a higher price tag and be more prone to breaking, given the aspect ratio that would be required. A number of factors impact the precision of the cut. The type of blade, in this case a drag knife, could impact the precision of the cut since the floating blade may not be rigid enough. The type of movement that is inherent to cutter plotters also impacts precision, as one of the axes is implemented by rolling the film against the blade.

The orientation of the pattern to be cut with respect to the cutter plotter thus becomes important. Lastly, accumulation of adhesive on the blade can effectively dull it, decreasing precision and increasing surface roughness due to discontinuous cutting and deposition of adhesive residues during the cut. A non-adherent blade, perhaps smoother or super hydrophobic, could help in this regard although the cost must always be considered.

The integral analysis of the results obtained with zigzag and curved and square serpentines emphasizes the importance of the equilibrium between the bonding strength of the adhesive to the cutting liner and the shear force exerted by the blade on the film. If the blade force overcomes the bonding strength the film moves, leading to dimensional error. The lateral force acting on the film is negligible when cutting straight lines but it increases when cutting slant straight lines (as in zigzags) and curved features, while it is most when implementing square serpentines (the blade suddenly turns onto the film). Hence, the smallest features can be achieved by cutting straight lines, preferably parallel to each other and not joined. Here, long straight channels of 200 μm width could be cut with 9.09% dimensional error and accuracy within 10 μm , as long as the channel is oriented parallel to the X axis of the cutter plotter and a 30° blade is used. Sharp aperture angles (30°) of narrow channels (300 μm) could be achieved in zigzags, a slanted straight line where the lateral force is expected to be minimal. The compromise between channel width and spacing between features becomes more strict when cutting serpentines, especially the square kind. In this case, a 300 μm -wide channel can only be achieved if the spacing between channels is 1.5 mm. Further conclusions obtained in this work include the existence of an optimal width of the PSA band surrounding a microfluidics network. A wider band than this optimal value does not lead to an increase of the pressure the network can handle. Finally, although the smallest feature that could be reliably cut in a number of geometries appears to be above 300 μm , this resolution is more than enough to address microliter, and even nanoliter, volumes. For example, a 400 μm -square chamber made in a 127 μm -thick film holds mere 20 nl. Smaller volumes could be implemented using thinner films. The patterning of stand-alone features such as posts, cages with characteristic dimension below few hundreds of micrometers is not deemed feasible using this technique due to the reasons indicated above. However, several applications with biological and chemical relevance have already been demonstrated using xurography, as detailed in the introduction. These applications rely on microfluidic networks similar to those studied here. The work presented here provides further guidelines for *a priori* design of robust microfluidics devices that can be rapidly and reliably manufactured using relatively inexpensive infrastructure and materials.

Acknowledgements

The authors thank Alicia Werner, Emily Wakefield and Madison Oldham of the Creative Inquiry program of Clemson University for discussion regarding the gradient generator.

References

- Ai Y, Beskok A, Gauthier DT, et al (2009) Dc Electrokinetic Transport of Cylindrical Cells in Straight Microchannels. *Biomicrofluidics* 3:44110. doi: 10.1063/1.3267095
- Alom Ruiz S, Chen CS (2007) Microcontact printing: A tool to pattern. *Soft Matter* 3:168. doi: 10.1039/b613349e
- Atencia J, Cooksey GA, Locascio LE (2012) A robust diffusion-based gradient generator for dynamic cell assays. *Lab Chip* 12:309. doi: 10.1039/c1lc20829b
- Bartholomeusz D, Boutté RW, Andrade JD (2005) Xurography: Rapid Prototyping of Microstructures Using a Cutting Plotter. *J Microelectromech Syst* 14:1364. doi: 10.1109/JMEMS.2005.859087
- Beebe DJ, Mensing G a, Walker GM (2002) Physics and applications of microfluidics in biology. *Annu Rev Biomed Eng* 4:261–86. doi: 10.1146/annurev.bioeng.4.112601.125916

- Bruzewicz D a, Reches M, Whitesides GM (2008) Low-cost printing of poly(dimethylsiloxane) barriers to define microchannels in paper. *Anal Chem* 80:3387–92. doi: 10.1021/ac702605a
- Carrilho E, Martinez AW, Whitesides GM (2009) Understanding wax printing: a simple micropatterning process for paper-based microfluidics. *Anal Chem* 81:7091–5. doi: 10.1021/ac901071p
- Cho C-H, Cho W, Ahn Y, Hwang S-Y (2007) PDMS–glass serpentine microchannel chip for time domain PCR with bubble suppression in sample injection. *J Micromechanics Microengineering* 17:1810–1817. doi: 10.1088/0960-1317/17/9/009
- Choi K, Ng AHC, Fobel R, Wheeler AR (2012) Digital microfluidics. *Annu Rev Anal Chem (Palo Alto Calif)* 5:413–40. doi: 10.1146/annurev-anchem-062011-143028
- Cosson S, Aeberli LG, Brandenberg N, Lutolf M (2015) Ultra-rapid prototyping of flexible, multi-layered microfluidic devices via razor writing. *Lab Chip* 15:72. doi: 10.1039/c4lc00848k
- Cubaud T, Ho C-M (2004) Transport of bubbles in square microchannels. *Phys Fluids* 16:4575. doi: 10.1063/1.1813871
- Dong Q, Xia Y, Whitesides GM (1996) Rapid Prototyping of Complex Structures with Feature Sizes Larger Than 20 micron. *Adv Mater* 8:917–919.
- Do J, Zhang JY, Klapperich CM (2011) Maskless writing of microfluidics: Rapid prototyping of 3D microfluidics using scratch on a polymer substrate. *Robotics and Computer-integrated Manufacturing* 27:245-248. doi: 10.1016/j.rcim.2010.06.004
- Duffy DC, McDonald JC, Schueller OJ, Whitesides GM (1998) Rapid Prototyping of Microfluidic Systems in Poly(dimethylsiloxane). *Anal Chem* 70:4974–84. doi: 10.1021/ac980656z
- Gorking R, Clime L, Madou M, Kido H (2010) Pneumatic pumping in centrifugal microfluidic platforms. *Microfluid Nanofluid* 9:541-549. doi: 10.1007/s10404-010-0571-x
- Greer J, Sundberg SO, Wittwer CT, Gale, BK (2007) Comparison of glass etching to xurography prototyping of microfluidic channels for DNA melting analysis. *J Micromech Microeng* 17:2407-2413. doi: 10.1088/0960-1317/17/12/003
- Harrison DJ, Manz A, Fan Z, et al (1992) Capillary Electrophoresis and Sample Injection Systems Integrated on a Planar Glass Chip. *Anal Chem* 64:1926–1932.
- Jaramillo MDC, Torrents E, Martínez-Duarte R, et al (2010) On-line separation of bacterial cells by carbon-electrode dielectrophoresis. *Electrophoresis* 31:2921–8. doi: 10.1002/elps.201000082
- Jiang XN, Zhou ZY, Yao J, et al (1995) Micro-fluid flow in microchannel. 8th Int. Conf. Solid State Sensors Actuators Eurosensors IX. pp 317–320
- Keenan TM, Folch A (2008) Biomolecular gradients in cell culture systems. *Lab Chip* 8:34–57. doi: 10.1039/b711887b
- Kido H, Micic M, Smith D, et al (2007) A novel, compact disk-like centrifugal microfluidics system for cell lysis and sample homogenization. *Colloids Surf B Biointerfaces* 58:44–51. doi: 10.1016/j.colsurfb.2007.03.015
- Martinez-Duarte R, Camacho-Alanis F, Renaud P, Ros A (2013) Dielectrophoresis of lambda-DNA using 3D carbon electrodes. *Electrophoresis* 34:1113–22. doi: 10.1002/elps.201200447

- Martinez-Duarte R, Gorkin R a, Abi-Samra K, Madou MJ (2010) The integration of 3D carbon-electrode dielectrophoresis on a CD-like centrifugal microfluidic platform. *Lab Chip* 10:1030–43. doi: 10.1039/b925456k
- Martinez-Duarte R, Madou MJ (2011) SU-8 Photolithography and Its Impact on Microfluidics. In: Chakraborty S, Mitra S (eds) *Microfluid. Nanofluidics Handb. Fabr. Implement. Appl.* CRC Press, pp 231–268
- Martinez-Duarte R, Renaud P, Madou MJ (2011) A novel approach to dielectrophoresis using carbon electrodes. *Electrophoresis* 32:2385–92. doi: 10.1002/elps.201100059
- Mernier G, Martinez-Duarte R, Lehal R, et al (2012) Very High Throughput Electrical Cell Lysis and Extraction of Intracellular Compounds Using 3D Carbon Electrodes in Lab-on-a-Chip Devices. *Micromachines* 3:574–581. doi: 10.3390/mi3030574
- Mu X, Zheng W, Sun J, et al (2013) Microfluidics for manipulating cells. *Small* 9:9–21. doi: 10.1002/smll.201200996
- Munson MS, Yager P A NOVEL MICROFLUIDIC MIXER BASED ON SUCCESSIVE LAMINATION. 7th Int. Conf. Miniaturized Chem. Biochem. Anal. Syst. Squaw Valley, California USA, pp 495–498
- Nath P, Maity TS, Petterson F, et al (2014) Polymerase chain reaction compatibility of adhesive transfer tape based microfluidic platforms. *Microsyst Technol* 20:1187-1193. doi: 10.1007/s00542-013-1901-1
- Pjescic I and Crews N (2012) Genotyping from saliva with a one-step microdevice. *Lab Chip* 12:2514-2519. doi: 10.1039/c2lc00010e
- Ren Y, Leung WW-F (2013) Flow and mixing in rotating zigzag microchannel. *Chem Eng J* 215-216:561–578. doi: 10.1016/j.cej.2012.09.136
- Rogers J a., Nuzzo RG (2005) Recent progress in soft lithography. *Mater Today* 8:50–56. doi: 10.1016/S1369-7021(05)00702-9
- Whitesides GM (2006) The origins and the future of microfluidics. *Nature* 442:368–73. doi: 10.1038/nature05058
- Wilding P, Pfahler J, Bau HH, et al (1994) Manipulation and flow of biological fluids in straight channels micromachined in silicon. *Clin Chem* 40:43–47.
- Woolley AT, Mathies RA (1994) Ultra-high-speed DNA fragment separations using microfabricated capillary array electrophoresis chips. *Proc. Natl. Acad. Sci. U. S. A.* pp 11348–11352
- Xia Y, Whitesides GM (1998) SOFT LITHOGRAPHY. *Annu Rev Mater Sci* 28:153–184.
- Xin Yi, Rimantas Kodzius, Xiuqing Gong, Kang Xiao WW (2010) A simple method of fabricating mask-free microfluidic.pdf. *Biomicrofluidics* 4:036503. doi: 10.1063/1.3487796
- Yuen PK, Goral VN (2010) Low-cost rapid prototyping of flexible microfluidic devices using a desktop digital craft cutter. *Lab Chip* 10:384–387. doi: 10.1039/b918089c